

STUDYING FAINT ULTRA HARD X-RAY EMISSION FROM AGN IN GOALS LIRGS WITH *SWIFT* BATMICHAEL KOSS¹, RICHARD MUSHOTZKY², WAYNE BAUMGARTNER³, SYLVAIN VEILLEUX^{2,3}, JACK TUELLER³, CRAIG MARKWARDT³, AND CAITLIN M. CASEY¹*Draft version February 6, 2013*

ABSTRACT

We present the first analysis of the all-sky *Swift* BAT ultra hard X-ray (14-195 keV) data for a targeted list of objects. We find the BAT data can be studied at $3\times$ fainter limits than in previous blind detection catalogs based on prior knowledge of source positions and using smaller energy ranges for source detection. We determine the AGN fraction in 134 nearby ($z < 0.05$) luminous infrared galaxies (LIRGs) from the GOALS sample. We find that LIRGs have a higher detection frequency than galaxies matched in stellar mass and redshift at 14-195 keV and 24-35 keV. In agreement with work at other wavelengths, the AGN detection fraction increases strongly at high IR luminosity with half of high luminosity LIRGs (50%, 6/12, $\log L_{\text{IR}}/L_{\odot} > 11.8$) detected. The BAT AGN classification shows 97% (37/38) agreement with *Chandra* and *XMM* AGN classification using hardness ratios or detection of a iron K-alpha line. This confirms our statistical analysis and supports the use of the *Swift* BAT all-sky survey to study fainter populations of any category of sources in the ultra hard X-ray band. BAT AGN in LIRGs tend to show higher column densities with $40 \pm 9\%$ showing 14-195 keV/2-10 keV hardness flux ratios suggestive of high or Compton-thick column densities ($\log N_{\text{H}} > 24 \text{ cm}^{-2}$), compared to only $12 \pm 5\%$ of non-LIRG BAT AGN. We also find that using specific energy ranges of the BAT detector can yield additional sources over total band detections with 24% (5/21) of detections in LIRGs at 24-35 keV not detected at 14-195 keV.

Subject headings: galaxies: active — X-rays

1. INTRODUCTION

The *Swift* BAT survey with over 500 AGN has revolutionized our study of the ultra hard X-ray sky (Tueller et al. 2010), but is still limited to bright ($F_{14-195} > 10^{-11} \text{ erg s}^{-1} \text{ cm}^{-2}$) objects in a blind survey. However, the stability of the instrument and the Gaussian nature of the noise, along with its wide energy range, allows the detection at fainter limits for a well defined, moderate sized sample of objects. For the first time, we use this property to study the AGN in luminous infrared galaxies (LIRGs; $\log L_{\text{IR}}/L_{\odot} > 11.0$).

The nature of the IR (8-1000 μm) emission and its relation to star formation in AGN is still not well understood. Past studies of samples of LIRGs have suggested, based primarily on optical and IR AGN indicators, that the dominant power source is star formation and AGN activity is more common in luminous sources (e.g. Veilleux et al. 1995). Recent studies used a variety of mid-IR spectral diagnostics and X-ray observations (Ptak et al. 2003; Teng et al. 2005; Veilleux et al. 2009; Teng & Veilleux 2010; Petric et al. 2011) to determine the AGN contribution. However, contamination from star formation and obscuration by dust and gas are problematic. Additionally, studies of AGN in the hard X-rays have shown the existence of large fraction of AGN not showing Spitzer IRAC AGN indicators (e.g. Donley et al. 2012) and some AGN are not optically detected (Koss et al. 2011a, 2012). Since a significant frac-

tion of X-ray selected AGN are in LIRGs (Koss et al. 2011b), an ultra-hard X-ray survey of LIRGs might come to different conclusions than those derived at lower energies.

The ultra hard X-rays ($> 15 \text{ keV}$) are much less sensitive to obscuration in the line-of-sight than soft X-ray or optical wavelengths and are biased only against highly Compton-thick AGN (Burlon et al. 2011). This band is also free from contamination from star formation that is significant in the soft X-rays ($< 5 \text{ keV}$). Additionally, in Compton-Thick AGN the radiation below 10 keV is almost completely absorbed in the X-rays whereas a broad Compton reflection hump appears in the $> 15 \text{ keV}$ continuum (Reynolds 1998). Thus, ultra-hard X-ray observations are an important complement to lower energy X-ray data.

We use the the most sensitive all-sky ultra hard X-ray survey from the *Swift* BAT instrument to search for AGN emission in LIRGs. Previous studies using the *INTEGRAL* satellite stacked emission from a large sample of IRAS bright galaxies and found no AGN detection (Walter & Cabral 2009). Additionally, past BAT AGN catalogs generated $> 4.8\sigma$ sources from "blind" detections (e.g. Tueller et al. 2010). To achieve higher sensitivities, we identify AGN (see §2.2) based on the prior knowledge of source positions and search in energy bands where we expect the AGN emission to be brightest. We adopt a standard cosmology ($\Omega_m = 0.3$, $\Omega_\Lambda = 0.7$, $H_0 = 70 \text{ km s}^{-1} \text{ Mpc}^{-1}$) to determine distances.

2. SAMPLE SELECTION AND DERIVED QUANTITIES

2.1. Sample of LIRGs and ULIRGs

We selected a sample of nearby LIRGs ($z < 0.05$) in the northern hemisphere (DEC > -25) from the Great Ob-

koss@ifa.hawaii.edu

¹ Institute for Astronomy, University of Hawaii, 2680 Woodlawn Drive, Honolulu, HI 96822, USA;² Astronomy Department, University of Maryland, College Park, MD, USA³ Astrophysics Science Division, NASA Goddard Space Flight Center, Greenbelt, MD, USA

servatories All Sky LIRG Survey (GOALS; Armus et al. 2009). In this redshift range, we are sensitive to X-ray luminosities of $L_{14-195 \text{ keV}} > 10^{42.0} \text{ erg/s}$. This limit effectively detects AGN since it is ten times larger than the maximum known emission from a starburst galaxy (e.g., M82, $\log L_{14-195 \text{ keV}} = 40.8 \text{ erg/s}$). Since single temperatures and SED templates can overestimate IR luminosities (Casey 2012), we recomputed GOALS IR luminosities based on SED fitting using IRAS data and a model joining a modified, single dust temperature greybody, that approximates hot-dust emission from AGN heating. We have limited our sources to be outside the Galactic plane ($b > 10^\circ$) because of source confusion in IRAS and Swift, as well difficulty measuring stellar masses because of high levels of optical extinction.

We have also limited our sample because in the low resolution BAT detector, source confusion from nearby bright AGN can occur. For blind source detection, Ajello et al. (2009) estimated a confusion radius of $5.5'$ at $\text{SNR}=2$, $3.8'$ at $\text{SNR}=3$, and $2.8'$ at $\text{SNR}=4$. We use a conservative approach and exclude all detections within $15'$ of BAT catalog sources. This excludes seven LIRGs from our study. NGC 232 and NGC 838 are in merging galaxy groups with a nearby ($<2'$) bright BAT-detected AGN companion. Additionally, UGC 3608 is $5.1'$ from a nearby ROSAT X-ray source, 1RXS J065711.8+462731. A 1.5 ks XRT observation suggests the majority of the flux is coincident with this ROSAT source. IRAS F03217+4022 and UGC 02717 are near a bright BAT AGN, IRAS 03219+4031 at $8.5'$ and $7'$ separation respectively. Finally, NGC 2524 is near a bright BAT AGN Mrk 0622 at $10.7'$. This leaves our total LIRG sample with 134 objects.

2.2. Faint BAT Source Detection in the GOALS Sample

In *Swift* BAT, the detector noise distribution is a Gaussian function centered at zero significance. Real astrophysical sources show a tail in the distribution at positive significances. Significant detections in the blind BAT detection catalogs are defined at $>4.8 \text{ SNR}$ to ensure zero false sources caused by random fluctuations in a large sample (≈ 500). Source detection is performed on a map weighted to the Crab Nebula, using a single average map of all eight energy bins between 14-195 keV.

However, many real astrophysical sources are below 4.8 SNR and can be studied based on known positions of galaxies and by studying energy range where the source population is brightest. Using the 24-35 keV energy bin for instance, we are more sensitive to the reflection component of obscured AGN. We use the *BATCELLDETECT* software which performs a sliding cell method to locate regions of the image which are significantly different from the background. We simultaneously fit all of the 1092 previously detected BAT AGN in the 70 month catalog along with the LIRGs in the 14-195 keV band and 24-35 keV band. Additionally, we select a comparison sample of 1000 galaxies matched in stellar mass and redshift from the NASA-Sloan Atlas (Blanton et al. 2011). To compute the stellar mass of the LIRGs and galaxy control sample, we use *ugriz* photometry following Koss et al. (2011b) using the software *kcorrect* v4.2 and SDSS imaging. For galaxies in close mergers, we follow Koss et al. (2010) and estimate the stellar mass from the largest galaxy.

We use the distribution of SNR for 1000 random pointings from the SDSS survey area to measure the significance of the X-ray detections in the other samples. The significance distribution at 14-195 keV of the random pointings is well fit by a Gaussian centered at $0.02 \pm 0.11 \text{ SNR}$ with $\sigma = 1.01 \pm 0.06$, consistent with the expected values for a Gaussian distribution of pure noise. For the LIRG and matched sample, the Gaussian distribution of noise is fit from the $\text{SNR} < 0$ source distribution.

We choose a 2.7σ cutoff SNR in the 134 LIRG sample to have on average less than one 'fake' noise source based on the Gaussian distribution of noise using both whole band 14-195 keV and 24-35 keV detections if we assume the distribution is pure noise. Finally, we note that the lowest SNR of any LIRG is -2.1 at 14-195 keV and -2.7 at 24-35 keV suggesting this cutoff should assure a sample of clean individual detections.

We also analyze X-ray emission using XSPEC v12.7.1 for the new sources between $2.7-4.8\sigma$. To calculate luminosities and upper limits, we assume an X-ray power law of $\Gamma=1.9$ and Galactic extinction, consistent with the mean 14-195 keV power law for Seyfert 2s in the 70 month blind detection catalog (Winter et al. 2009). The BAT emission is absorbed by $<10\%$ for $N_H < 3 \times 10^{23} \text{ cm}^{-2}$, but sources with larger obscurations are underestimated. To determine 1σ errors in luminosity, we include the error from assuming a fixed power law index (14%) as well as sky and detector noise ($<37\%$). Finally, to better understand the average properties of the sources, we fit a simple X-ray power law to the average emission in each X-ray band.

2.3. X-ray Hardness Flux Ratios and Comparison Sample

The ultra hard X-ray hardness flux ratio ($HR_{UX} = 14-195 \text{ keV}/2-10 \text{ keV}$) provides a measure of obscuration in heavily obscured AGN ($N_H > 10^{23} \text{ cm}^{-2}$) since the transmitted hard X-ray emission is suppressed by a much larger factor than the ultra hard X-ray emission. Long term AGN variability can affect this ratios, but this variability is typically 20-40% in the 2-10 keV X-rays (McHardy 2001) and smaller in the ultra hard X-rays (Ricci et al. 2011).

To estimate absorbing columns corresponding to HR_{UX} , we use the MYTorus model (Murphy & Yaqoob 2009), which fully treats photoelectric absorption and relativistic Compton scattering. The intrinsic AGN emission was modeled as a power law ($\Gamma=1.9$) and the column density assumes the torus is seen edge-on following Burlon et al. (2011). In this model, the emission is reduced by four at $N_H = 3 \times 10^{23} \text{ cm}^{-2}$ and $N_H = 4 \times 10^{24} \text{ cm}^{-2}$ for 2-10 keV and 14-195 keV, respectively, showing that the ultra hard X-rays can pass through an order of magnitude higher absorbing column.

Finally, as a comparison sample we measured the HR_{UX} from 49 non-LIRG BAT-detected AGN ($\log L_{IR}/L_\odot < 11.0$) from Winter et al. (2009) from the same redshift range to understand whether BAT AGN in LIRGs have higher levels of obscuration.

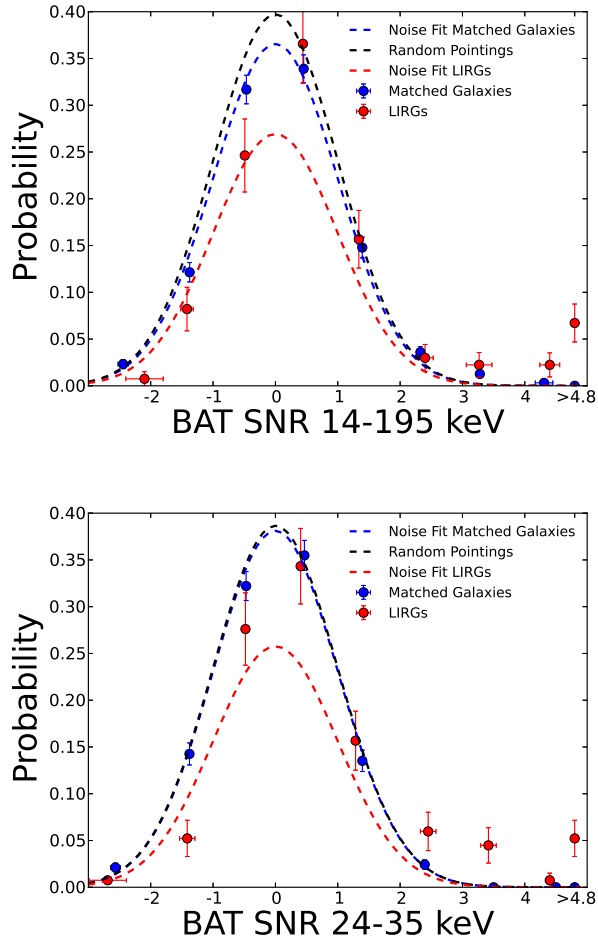


FIG. 1.— Histogram of mean BAT signal to noise ratios (SNR) for the LIRGs and a sample matched in stellar mass and redshift for 14-195 keV (left) and 24-35 keV (right). The dashed lines indicate the best fit lines for the expected Gaussian noise in each sample. The black dashed lines indicate the expected distribution from random pointings. Error bars are computed from 1,000 bootstrapping trials. The LIRG sample has a higher detection frequency than the matched galaxy sample and random pointings.

3. RESULTS

3.1. The Fraction of AGN in U/LIRGs

We compare the BAT detection significance at 14-195 keV and 24-35 keV of the LIRGs and a sample of galaxies matched in stellar mass and redshift (Fig. 1). There is an excess of LIRGs at SNR >3 for 14-195 keV and SNR >2 at 24-35 keV, based on the distributions from random pointings. There is an excess of LIRG detections over the matched galaxies at SNR >4 at 14-195 keV and at SNR >2 at 24-35 keV. The fraction in the LIRG sample above 2.7σ at 14-195 keV is $11\% \pm 2$ (16/134) and at 24-35 keV $14\% \pm 2$ (19/134), while the matched galaxy sample is only $2\% \pm 1$ (21/1000) at 14-195 keV and $1\% \pm 1$ (5/1000) at 24-35 keV. This suggests that LIRGs are more likely to be detected as ultra hard X-ray AGN than galaxies of a similar stellar mass and redshift consistent with previous results (e.g. Koss et al. 2011b). Although we cannot reliably identify individual sources below 2.7 SNR, analysis of Gaussian fits to the negative SNR distribution representative of noise, show a total LIRG sample

detection fraction of $33\% \pm 8\%$ at 14-195 keV and $36\% \pm 7\%$ at 24-35 keV compared to the matched galaxy sample detection fraction of only $9\% \pm 2\%$ at 14-195 keV and $4\% \pm 1\%$ at 24-35 keV.

We also analyze the average emission in each BAT energy band (Fig. 2). We find there is a significant excess among stacked sources at >1 SNR, between energies of 14-150 keV (Fig. 2-left). For the >4.8 SNR sources, we find they are fit by a power law with index $\Gamma = 2.18 \pm 0.30$ and for the sources above the cutoff ($2.7 < \text{SNR} < 4.8$), we find a harder spectrum of $\Gamma = 1.51 \pm 0.22$ (Fig. 2-right).

We also look for additional sources detected in the 24-35 keV band where the reflection component of Compton Thick AGN is expected to contribute significantly that are not detected in the 14-195 keV band. Of the 12 new SNR = 2.7-4.8 detections, five are detected in the 14-195 keV band with a stronger significance than the 24-35 keV, and the remaining 7 are detected with stronger significances in the 24-35 keV band. More than half (12/21, 57%) of detected LIRGs are at SNR = 2.7-4.8 and thus not detected in previous BAT catalogs.

The BAT detection fraction of LIRGs at 24-35 and 14-195 keV is shown in Figure 3. The AGN detection fraction increases strongly at high IR luminosity ($\log L_{\text{IR}}/L_{\odot} > 11.8$) with half 50% (6/12) detected above 2.7 SNR.

3.2. Comparison with 2-10 keV Classification

We compare the AGN classification using *Chandra* and *XMM-Newton* of previous LIRG samples based on hardness ratios of the X-ray spectra ($\text{HR} > -0.3$) or the detection of an Fe K α line with the BAT classification. The C-GOALS *Chandra* survey (Iwasawa et al. 2011) classified luminous LIRGs ($L_{\text{IR}} > 11.73$). The BAT and *Chandra* classifications agree for 18/19 galaxies common in both samples. VV 340a, a Compton-thick AGN is detected in C-GOALS, but not in BAT (SNR = 0.57). More nearby studies of less luminous LIRGs were done by Lehmer et al. (2010) and Pereira-Santaella et al. (2011) using *Chandra* and *XMM-Newton*. We find agreement with BAT in 20/20 cases in these samples. Overall we find agreement in 38/39 cases or 97% based on hardness ratios or the detection of an Fe K α line. There are other cases where a lower luminosity AGN is detected using the ratio of the galaxy nucleus to total galaxy emission in the 2-8 keV band (NGC 4194, NGC 7771; Lehmer et al. 2010) that are not detected as AGN in BAT.

We also compare the AGN classification for 12 new SNR = 2.7-4.8 detections. Five of these sources are detected in the 14-195 keV band with a stronger significance than the 24-35 keV, and 7 are detected with stronger significances in the 24-35 keV band. NGC 7674, UGC 5101, NGC 6926, UGC 08696 (Mrk 273), UGC 08058 (Mrk 231), NGC 3690 are Compton Thick (Severgnini et al. 2012) IRAS F17207-0014 shows the presence of strong (at 2σ), high-ionization Fe K line on a hard continuum Iwasawa et al. (2011). UGC 2608 is also listed as a heavily obscured Compton-Thick AGN ($N_{\text{H}} > 10^{24} \text{ cm}^{-2}$, Guainazzi et al. 2005). A *Chandra* observation of NGC 1961 has a hardness ratio indicative of an AGN ($\text{HR} = -0.2$). Mrk 331 has a hardness flux ratio indicative of star formation ($\text{HR} = -0.5$), no significant Fe K line, weak 2-10 keV emission ($\log L_{2-10 \text{ keV}} = 40.7$),

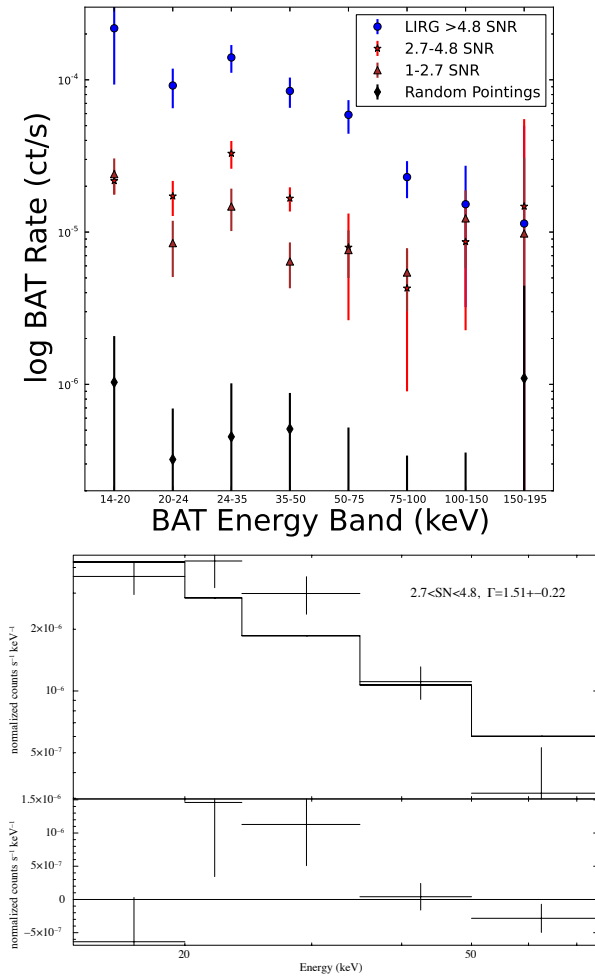


FIG. 2.— *Left*: Stacked count rates in each of the 8 BAT energy bands. We find an excess of emission for sources above 1σ for energies 14–150 keV. *Right*: Stacked spectra for sources between $2.7 < \text{SNR} < 4.8$ with residuals shown. A fit with a simple power law has a best fit of $\Gamma = 1.51 \pm 0.22$, consistent with the power law of other BAT sources. Residual emission is found at 20–35 keV, consistent with fact that 8/9 of the sources with high quality X-ray data are Compton Thick AGN.

however it does have a compact radio source suggesting an AGN Parra et al. (2010). IRAS F02437+2122 has no high quality X-ray data, but is a LINER AGN (Veilleux et al. 1995). UGC 3094 has a Ne V detection suggesting the presence of an AGN Petric et al. (2011). Finally, NGC 0877 has no high quality observation to test for the presence of an AGN.

3.3. Comparison with Spitzer AGN Classification

The Ne V lines at 14.3 and 24.3 μm imply the presence of an AGN since this line requires 97 eV and is too large to be produced even by O stars. There are 29 LIRGs with Ne V detections overlapping in our sample with the Petric et al. (2011) Spitzer study (Table 1), with 14/29 (48%) detected in BAT. Conversely, 14/21 (67%) of BAT-detected LIRGs have Ne V. The 33% non-detection in Ne V for BAT-detected LIRGs is lower than the 10% found by Weaver et al. (2010) for all BAT AGN. However, this study use a deeper exposure map which is more sensitive to fainter sources (70 vs. 9 months),

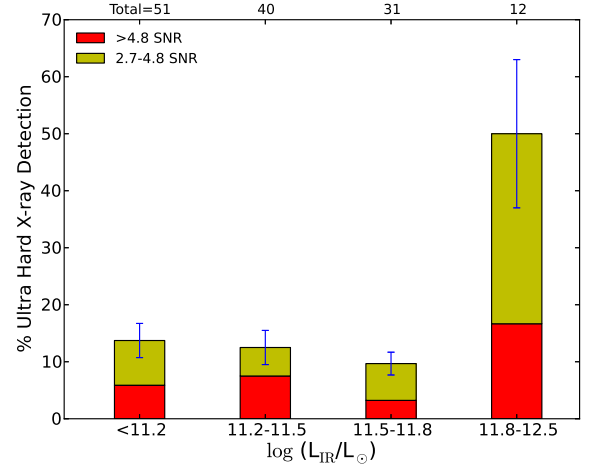


FIG. 3.— *Left*: GOALS LIRGs IR luminosity by BAT SNR. We find a higher fraction of detections at the highest IR luminosity. Error bars are based on statistical error assuming poisson statistics. The trend is in agreement with previous emission line diagnostics work (e.g. Veilleux et al. 1995).

as well as fainter detection limits ($2.7 < \text{SNR} < 4.8$), and is exclusively of LIRGs which may be more likely to have optically thick, dusty gas close to the AGNs (e.g., Armus et al. 2007). We note that 5/6 of the sources without Ne V detections have X-ray, optical, or radio observations confirming the presence of AGN (see §3.2).

3.4. Properties of AGN in LIRGs Compared to non-LIRGs

Previous hard X-ray observations have found some LIRGs to be heavily obscured Compton-thick AGN (Komossa 2008; della Ceca et al. 2002; Imanishi et al. 2003, NGC 6240, NGC 3690, UGC 5101). We measure HR_{UX} to test whether LIRGs are more obscured than non-LIRG BAT AGN (Fig. 4-right). The median $HR_{UX} = 15$ among LIRGs corresponds to a $N_H \approx 4 \times 10^{23} \text{ cm}^{-2}$ compared to a median $HR_{UX} = 3.8$ or $N_H \approx 7 \times 10^{22} \text{ cm}^{-2}$ for non-LIRG BAT AGN. A Kolmogorov-Smirnov (K-S) test indicates a ($< 1\%$) chance that the HR_{UX} from the samples are from the same distribution indicating that LIRGS show systematically higher column densities.

4. SUMMARY AND DISCUSSION

We search for nuclear activity in nearby LIRGs based on the detection of ultra high X-ray emission from Swift BAT. We find:

- (i) A lower cutoff ($\text{SNR} > 2.7$) than previous ‘blind’ catalogs ($\text{SNR} > 4.8$) can be used for a moderate sample size (≈ 100). Using this cutoff at 14–195 keV and 24–35 keV, we find agreement in AGN classification for 38/39 cases (97%) from Chandra and XMM based on hardness ratios or the detection of an Fe $K\alpha$ line.
- (ii) We find that using specific energy ranges of the BAT detector can yield additional sources over single band detections with 24% (5/21) of detections in LIRGs at 24–35 keV not detected at 14–195 keV.

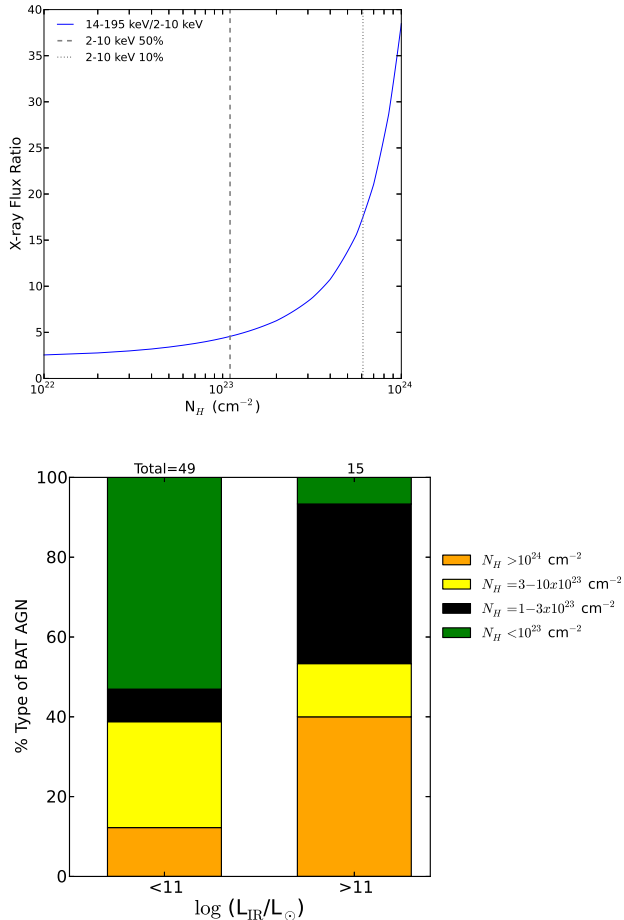


FIG. 4.— *Left*: Ultra hard X-ray hardness flux ratio ($HR_{UX} = 14-195 \text{ keV}/2-10 \text{ keV}$) for an AGN with a power-law spectrum index of 1.9, as a function of the column density of the torus as seen edge-on. This measure provides a measure of obscuration since the transmitted hard X-ray emission is suppressed by a much larger factor than the ultra hard X-ray emission. *Right*: Approximate column density from HR_{UX} as a function of IR luminosity. BAT-selected AGN in LIRGs tend to show higher column densities than non-LIRG AGN.

Of the 12 new SNR=2.7-4.8 detections, 7 are detected with stronger significances in the 24-35 keV band than the 14-195 keV band.

- (iii) LIRGs have a higher BAT-detection frequency at 14-195 keV and 24-35 keV compared to galaxies

matched in stellar mass. Additionally, the BAT-detection fraction increases strongly at high IR luminosities with half of high luminosity LIRGs detected (50%, 6/12, $\log L_{IR}/L_{\odot} > 11.8$).

- (iv) BAT detected AGN in LIRGs have higher column densities with $40 \pm 9\%$ (6/15) having HR_{UX} suggestive of high column densities ($\log N_H > 24 \text{ cm}^{-2}$), compared to only $12 \pm 5\%$ (6/49) of non-LIRG BAT AGN. Additionally, 8/9 of the new SNR=2.7-4.8 BAT sources with high quality X-ray data are Compton-Thick based on past observations. We also find the stack spectra of these new sources show an excess at 24-35 keV consistent with a reflection component in a Compton-thick AGN.

We note that there are several LIRGs in warm infrared sources detected in the ultra hard X-rays (i.e. UGC 07064, MCG +08-11-011, NGC 5995, Mrk 520, NGC 1142, Mrk 463) that are not included in the GOALS sample because of the $60 \mu\text{m}$ cutoff, therefore this study underestimate the total fraction of AGN in all LIRGs based on the ultra hard X-rays. These sources are predominantly unobscured Seyfert 1s where the AGN contributes significantly to the total IR emission and will be discussed in a forthcoming paper.

These results show the potential to use the *Swift* BAT all-sky survey to study $\approx 3\times$ fainter populations of ultra hard X-ray sources than the past catalogs based on source positions and by using certain energy ranges where the sources are expected to be brightest. A different survey could study faint BAT-detection in obscured AGN, star forming galaxies, radio loud AGN, or galactic sources. Additionally, since lower energy all-sky surveys such as ROSAT show little or no correlation in count rates with *Swift* because of the effects of obscuration (Markwardt et al. 2005), this remains an important all-sky resource to utilize with small field of view X-ray missions. For instance, this technique could be used to identify promising candidates to study with higher sensitivity and resolution small field of view missions such as *NuSTAR* and *Astro-H*.

The success of *Swift* in identifying similar numbers of AGN in nearby LIRGs ($z < 0.05$) as *Chandra* and *XMM* suggests that higher sensitivity missions such as *NuSTAR* and *Astro-H* hold great promise to study even more distant, obscured AGN ($z > 0.05$, $N_H > 10^{24} \text{ cm}^{-2}$) since they can reach these all-sky sensitivities in only 15 minutes.

5. ACKNOWLEDGEMENTS

We acknowledge the *Swift* BAT team and are grateful to Ezequiel Treister and Marco Ajello for discussion and suggestions.

REFERENCES

- Ajello, M., et al. 2009, *The Astrophysical Journal*, 690, 367
- Armus, L., et al. 2007, *The Astrophysical Journal*, 656, 148
- . 2009, *Publications of the Astronomical Society of the Pacific*, 121, 559
- Blanton, M. R., Kazin, E., Muna, D., Weaver, B. A., & Price-Whelan, A. 2011, *The Astronomical Journal*, 142, 31
- Burlon, D., Ajello, M., Greiner, J., Comastri, A., Merloni, A., & Gehrels, N. 2011, *The Astrophysical Journal*, 728, 58
- Casey, C. M. 2012, eprint arXiv, 1206, 1595
- della Ceca, R., et al. 2002, *The Astrophysical Journal*, 581, L9
- Donley, J. L., et al. 2012, *The Astrophysical Journal*, 748, 142
- Greenhill, L. J., Tilak, A., & Madejski, G. 2008, *The Astrophysical Journal*, 686, L13
- Guainazzi, M., Matt, G., & Perola, G. C. 2005, *Astronomy and Astrophysics*, 444, 119
- Imanishi, M., Terashima, Y., Anabuki, N., & Nakagawa, T. 2003, *The Astrophysical Journal*, 596, L167
- Iwasawa, K., et al. 2011, *Astronomy and Astrophysics*, 529, 106
- Komossa, S. 2008, *The Nuclear Region*, 32, 86

- Koss, M., et al. 2011a, The Astrophysical Journal Letters, 735, L42
- Koss, M., Mushotzky, R., Treister, E., Veilleux, S., Vasudevan, R., & Tripp, M. 2012, The Astrophysical Journal, 746, L22
- Koss, M., Mushotzky, R., Veilleux, S., & Winter, L. 2010, The Astrophysical Journal Letters, 716, L125
- Koss, M., Mushotzky, R., Veilleux, S., Winter, L. M., Baumgartner, W., Tueller, J., Gehrels, N., & Valencic, L. 2011b, The Astrophysical Journal, 739, 57
- Lehmer, B. D., Alexander, D. M., Bauer, F. E., Brandt, W. N., Goulding, A. D., Jenkins, L. P., Ptak, A., & Roberts, T. P. 2010, The Astrophysical Journal, 724, 559
- Markwardt, C. B., Tueller, J., Skinner, G. K., Gehrels, N., Barthelmy, S. D., & Mushotzky, R. F. 2005, The Astrophysical Journal, 633, L77
- McHardy, I. M. 2001, Probing the Physics of Active Galactic Nuclei, ASP Conference Proceedings, ISBN: 1-58381-056-0, 224, 205
- Murphy, K. D., & Yaqoob, T. 2009, Monthly Notices of the Royal Astronomical Society, 397, 1549
- Parra, R., Conway, J. E., Aalto, S., Appleton, P. N., Norris, R. P., Pihlström, Y. M., & Kewley, L. J. 2010, The Astrophysical Journal, 720, 555
- Pereira-Santaella, M., et al. 2011, Astronomy and Astrophysics, 535, 93
- Petric, A. O., et al. 2011, The Astrophysical Journal, 730, 28
- Ptak, A., Heckman, T., Levenson, N. A., Weaver, K., & Strickland, D. 2003, The Astrophysical Journal, 592, 782
- Ricci, C., Walter, R., Courvoisier, T. J. L., & Paltani, S. 2011, Astronomy and Astrophysics, 532, 102
- Severgnini, P., Caccianiga, A., & della Ceca, R. 2012, Astronomy and Astrophysics, 542, 46
- Teng, S. H., & Veilleux, S. 2010, The Astrophysical Journal, 725, 1848
- Teng, S. H., Wilson, A. S., Veilleux, S., Young, A. J., Sanders, D. B., & Nagar, N. M. 2005, The Astrophysical Journal, 633, 664
- Tueller, J., et al. 2010, The Astrophysical Journal Supplement, 186, 378
- Veilleux, S., et al. 2009, The Astrophysical Journal, 701, 587
- Veilleux, S., Kim, D.-C., Sanders, D. B., Mazzarella, J. M., & Soifer, B. T. 1995, Astrophysical Journal Supplement v.98, 98, 171
- Walter, R., & Cabral, N. 2009, Astronomy and Astrophysics, 497, 97
- Weaver, K. A., et al. 2010, The Astrophysical Journal, 716, 1151
- Winter, L. M., Mushotzky, R. F., Reynolds, C. S., & Tueller, J. 2009, The Astrophysical Journal, 690, 1322

TABLE 1 Properties of GOALS LIRGs

Galaxy Name	L_{IR}^1 log L_\odot	SNR ² 14-195 keV	SNR 24-35 keV	$L_{14-195\text{ keV}}^3$ log erg/s	HR $_{UX}^4$ Diag	NeV ⁵ X-ray	X-ray ⁶ Ref
BAT Detections							
IRAS F02437+2122	11.13	0.7	2.7	<42.9	?		
IRAS F05189-2524	12.14	6.0	4.2	43.72 $^{+0.12}_{-0.09}$	4	Y	I11
IRAS F17207-0014	12.36	1.1	3.3	<43.6	?		
MCG-03-34-064	11.13	12.8	7.3	43.25 $^{+0.05}_{-0.05}$	15	Y	W09
MCG+04-48-002	10.84	26.8	16.4	43.54 $^{+0.02}_{-0.02}$	26	Y	W09
MRK 0331	11.42	1.9	2.7	<42.6	?		
NGC 0877	10.99	2.3	3.2	<42.4	?		
NGC 1068	11.37	15.6	11.6	42.03 $^{+0.04}_{-0.04}$	99	Y	L10
NGC 1275	11.25	50.2	19.5	43.69 $^{+0.01}_{-0.01}$	6		P06
NGC 1961	10.87	2.3	2.9	<42.4	?		
NGC 3690	11.76	2.9	3.0	42.04 $^{+0.27}_{-0.17}$	10		I11
NGC 6240	11.81	18.8	13.8	43.96 $^{+0.03}_{-0.03}$	29	Y	I11
NGC 6926	11.17	2.8	3.6	42.81 $^{+0.3}_{-0.18}$	126	Y	G08
NGC 7469	11.57	28.5	16.6	43.61 $^{+0.02}_{-0.02}$	2	Y	W09
NGC 7674	11.56	4.2	2.7	43.28 $^{+0.18}_{-0.12}$	20	Y	L10
NGC 7679	11.05	6.5	3.8	43.01 $^{+0.11}_{-0.08}$	5	Y	P11
PGC 016795	11.20	9.3	6.3	43.25 $^{+0.07}_{-0.06}$	38	Y	XRT
UGC 03094	11.38	3.1	1.6	43.05 $^{+0.26}_{-0.16}$?	Y	
UGC 05101	11.96	4.8	3.6	43.43 $^{+0.15}_{-0.11}$	53	Y	I11
UGC 08058 (Mrk 231)	12.50	3.7	1.5	43.34 $^{+0.21}_{-0.14}$	7	Y	I11
UGC 08696 (Mrk 273)	12.11	4.4	2.4	43.31 $^{+0.17}_{-0.12}$	8	Y	I11
BAT Non-Detections							
IRAS 04271+3849	11.14	2.2	0.5	<42.9		Y	
NGC 5256	11.47	1.9	2.2	<42.9			
NGC 4418	10.99	1.8	1.3	<43.2			
IRAS 18090+0130	11.56	1.8	-0.5	<43.2			
IC 5298	11.57	1.7	-0.1	<43.0			
MCG -02-33-098	11.01	1.5	1.0	<42.6			
NGC 5104	11.10	1.5	0.4	<42.7			
ESO 557-G002	11.11	1.4	1.5	<42.8			
NGC 5990	10.96	1.3	-0.1	<43.1			
UGC 02982	11.14	1.2	1.3	<42.7		Y	
NGC 6621	11.17	1.2	0.7	<42.7			
ESO 550-IG025	11.44	1.2	0.3	<42.8			
IRAS 17578-0400	11.26	1.1	1.4	<42.5			
MCG+02-20-003	11.03	1.1	0.8	<42.6			
PGC 061152	11.06	1.1	-0.4	<42.8			
IRAS 05083+2441	11.22	1.1	-1.0	<43.7			
NGC 0034	11.48	1.1	0.0	<42.8			
IRAS 23436+5257	11.50	1.1	0.8	<42.6			
IRAS F03359+1523	11.51	1.0	1.3	<42.8			

TABLE 1 – Continued

Galaxy Name	L_{IR}^1 $\log L_{\odot}$	SNR ² 14-195 keV	SNR 24-35 keV	$L_{14-195\text{ keV}}^3$ $\log \text{erg/s}$	HR _{UX} ⁴ Diag	NeV ⁵ X-ray	X-ray ⁶ Ref
IRAS F16516-0948	11.25	1.0	1.2	<43.1			
NGC 5010	10.75	0.9	0.3	<42.7			
NGC 7771	11.31	0.8	2.0	<42.4			
MCG-03-04-014	11.62	0.8	0.9	<42.6			
PGC 061675	11.08	0.8	0.1	<42.8			
IRAS F16399-0937	11.48	0.8	-0.1	<43.2			
NGC 5331	11.53	0.8	-0.6	<43.0			
ESO 593-IG008	11.86	0.7	1.8	<42.9			
NGC 2146	10.75	0.7	-1.0	<43.0			
IC 0860	11.05	0.7	0.3	<42.3			
NGC 3110	11.20	0.7	0.1	<42.6			
UGC 02238	11.29	0.7	0.1	<42.8		Y	
UGC 04881	11.64	0.7	0.0	<43.2			
NGC 0023	11.04	0.6	1.7	<42.5			
NGC 2623	11.51	0.6	1.3	<42.7		Y	
MCG +01-42-008	11.35	0.6	0.8	<43.1			
UGC 08739	11.02	0.6	-0.2	<42.5			
IRAS 05442+1732	11.25	0.6	0.4	<43.3			
IRAS F16164-0746	11.50	0.6	0.3	<43.2			
VV 340a	11.64	0.6	-0.1	<42.2			
UGC 01845	11.08	0.5	0.9	<42.5			
VV 250a	11.74	0.5	0.8	<43.0			
NGC 5257	11.37	0.5	0.7	<42.9		Y	
ESO 507-G070	11.40	0.5	0.1	<42.9			
MCG+07-23-019	11.54	0.5	-0.3	<43.3			
NGC 0695	11.65	0.5	-0.7	<42.6			
IC 0564	11.13	0.4	1.0	<42.8			
NGC 6090	11.50	0.4	-0.2	<43.0			
IRAS F05187-1017	11.25	0.3	1.1	<43.1			
NGC 4194	10.90	0.3	1.0	<42.6			
NGC 1797	11.00	0.3	1.0	<42.5			
UGC 11041	10.98	0.3	0.5	<43.0			
NGC 1614	12.29	0.3	0.4	<42.5			
IRAS 03582+6012	11.37	0.3	-0.6	<42.6		Y	
II Zw 096	11.90	0.2	1.5	<42.3			
MCG+12-02-001	11.45	0.2	1.4	<42.5		Y	
UGC 08387	11.58	0.2	1.0	<42.4			
NGC 0317B	11.17	0.2	0.5	<42.6			
NGC 0992	11.00	0.2	0.3	<42.4			
PGC 014069	11.14	0.2	0.1	<42.9			
NGC 6286	11.26	0.2	-1.2	<42.6			
IRAS F06076-2139	11.61	0.2	0.2	<43.3			
NGC 7592	11.36	0.1	1.1	<43.0			
NGC 3221	10.97	0.1	0.4	<42.7			
Mrk 1490	11.30	0.1	-0.2	<42.8			
NGC 0828	11.31	0.1	-1.9	<42.6			
MCG -02-01-052	11.45	0.0	0.6	<41.9			
PGC 054330	11.14	0.0	-0.6	<42.4			
IRAS F12224-0624	11.20	0.0	-0.1	<43.0			
NGC 4922	11.28	-0.1	2.0	<42.8		Y	
NGC 2342	11.05	-0.1	0.8	<42.7			
IRAS 05223+1908	11.57	-0.1	0.7	<42.5			
NGC 6701	11.00	-0.1	0.4	<42.3			
NGC 6670	11.59	-0.1	0.4	<43.0			
NGC 5395	10.68	-0.1	0.1	<42.3			
IC 4280	10.98	-0.2	0.2	<42.5			
UGC 01385	11.00	-0.2	-0.5	<42.7			
NGC 5936	10.96	-0.3	-0.5	<42.8		Y	
NGC 5653	10.93	-0.4	0.6	<43.0			
ESO 602-G025	11.30	-0.4	0.4	<43.0			
NGC 6052	10.88	-0.4	-0.1	<42.8			
VV 283	11.53	-0.4	-0.2	<41			
IC 2810	11.05	-0.4	-0.8	<42.5			
IRAS F17138-1017	11.37	-0.4	-1.2	<42.8			
IRAS F01364-1042	11.77	-0.4	-0.8	<42.9			
NGC 6907	10.91	-0.5	0.1	<43.2			
UGC 03410	10.93	-0.5	-0.6	<43.0			
MCG+08-18-013	11.28	-0.5	-1.0	<42.9			
IC 1623A	11.67	-0.5	-1.1	<42.8			
IRAS F08339+6517	11.04	-0.6	-0.1	<42.6			
MCG+08-11-002	11.38	-0.6	-0.4	<42.9			
NGC 7752/3	10.84	-0.6	-0.6	<42.6			
NGC 2388	11.11	-0.6	-0.8	<42.4		Y	
NGC 6786	11.27	-0.7	-0.7	<42.9			
UGC 03351	11.27	-0.8	0.5	<42.6			
UGC 09913	12.13	-0.8	0.3	<42.7			
IRAS F10173+0828	11.75	-0.8	-0.3	<42.5			

TABLE 1 – Continued

Galaxy Name	L_{IR}^1 $\log L_\odot$	SNR ² 14-195 keV	SNR 24-35 keV	$L_{14-195\text{ keV}}^3$ $\log \text{ erg/s}$	HR_{UX}^4 Diag	NeV ⁵ X-ray	X-ray ⁶ Ref
IRAS 20351+2521	11.56	-0.9	0.5	<42.6			
NGC 7591	11.04	-0.9	0.0	<42.6			
MCG +00-29-023	11.26	-0.9	-0.7	<42.9			
UGC 12150	11.29	-0.9	-1.3	<42.8			
IRAS 05129+5128	11.40	-1.0	-1.9	<43.1			
MCG +02-04-025	11.66	-1.1	0.5	<43.0			
NGC 0958	11.13	-1.1	0.1	<42.7			
IRAS 21101+5810	11.72	-1.2	0.1	<43.1			
MCG+05-06-036	11.60	-1.2	-0.2	<43.2			
NGC 5734	10.94	-1.2	-0.9	<43.2			
UGC 02369	11.70	-1.3	1.0	<41.8			
IC 0214	11.39	-1.4	-0.5	<42.2			
III Zw 035	11.60	-1.6	-0.3	<43.0			
IRAS F10565+2448	11.99	-1.7	-1.0	<43.3			
VV 705	12.33	-1.8	0.6	<42.7		Y	
PGC 070417	11.31	-2.0	-1.3	<42.9			
MCG -01-60-022	11.16	-2.1	-2.7	<42.9			

¹ IR luminosity ($L_{8-1000\text{ }\mu\text{m}} > 10^{11} L_\odot$) based on SED fitting (Casey 2012) using data from IRAS.

² BAT Signal to Noise Ratio (SNR) defined as the background-subtracted source count rate divided by local background standard deviation.

³ BAT luminosity and 1σ error. Lower limits were calculated at 3σ , using an X-ray power law of $\Gamma=1.9$, and Galactic extinction, consistent with the mean 14-195 power law for Seyfert 2s in the

BAT sample (Winter et al. 2009).

⁴ Ultra hard X-ray hardness flux ratio ($HR_{UX}=14-195\text{ keV}/2-10\text{ keV}$).

⁵ Presence of NeV from Petric et al. (2011).

⁶ 2-10 keV references where G08=Greenhill et al. (2008), I11=Iwasawa et al. (2011), L10=Lehmer et al. (2010), P11=Pereira-Santaella et al. (2011), W09=Winter et al. (2009)

⁷ ? indicates no available high quality 2-10 keV measurement.